Effects of wall electrodes on Hall effect thruster plasma

S. Langendorf, K. Xu, and M. Walker

Citation: Physics of Plasmas (1994-present) **22**, 023508 (2015); doi: 10.1063/1.4908273
View online: http://dx.doi.org/10.1063/1.4908273
View Table of Contents: http://scitation.aip.org/content/aip/journal/pop/22/2?ver=pdfcov
Published by the AIP Publishing

Effects of wall electrodes on Hall effect thruster plasma

S. Langendorf,[1,2,a)] K. Xu,[3,b)] and M. Walker[1,2,c)]
[1]School of Aerospace Engineering, Georgia Institute of Technology, Atlanta, Georgia 30332, USA
[2]High-Power Electric Propulsion Laboratory, 625 Lambert St NW, Atlanta, Georgia 30318, USA
[3]School of Mechanical and Aerospace Engineering, University of Alabama in Huntsville, Huntsville, Alabama 35899, USA

(Received 20 February 2014; accepted 29 January 2015; published online 13 February 2015)

This paper investigates the physical mechanisms that cause beneficial and detrimental performance effect observed to date in Hall effect thrusters with wall electrodes. It is determined that the wall electrode sheath can reduce ion losses to the wall if positioned near the anode (outside the dense region of the plasma) such that an ion-repelling sheath is able to form. The ability of the wall electrode to form an ion-repelling sheath is inversely proportional to the current drawn—if the wall electrode becomes the dominant sink for the thruster discharge current, increases in wall electrode bias result in increased local plasma potential rather than an ion-repelling sheath. A single-fluid electron flow model gives results that mimic the observed potential structures and the current-sharing fractions between the anode and wall electrodes, showing that potential gradients in the presheath and bulk plasma come at the expense of current draw to the wall electrodes. Secondary electron emission from the wall electrodes (or lack thereof) is inferred to have a larger effect if the electrodes are positioned near the exit plane than if positioned near the anode, due to the difference in energy deposition from the plasma. © *2015 AIP Publishing LLC*.
[http://dx.doi.org/10.1063/1.4908273]

I. INTRODUCTION

Hall effect thrusters (HETs) are plasma-based propulsion devices used for in-space orbit maintenance and orbit raising of satellites and spacecraft. HETs offer an order of magnitude increase in specific impulse over chemical rockets due to their ability to couple external electrical power to the ionized propellant.[1] Fig. 1 shows a schematic of a typical HET. In the HET discharge plasma, electrons carry current from the cathode to the anode. A primarily radial applied magnetic field traps electrons in a closed drift path within the thruster discharge channel. This azimuthal ExB drift around the annular discharge channel is the Hall current for which the thruster is named.

The magnetic field of HETs is the important feature that makes them effective for propulsion; the restriction of electron mobility perpendicular to the magnetic field allows the plasma to sustain much higher electric fields at a given discharge current than would be otherwise possible. The HET plasma is also quasineutral, which is advantageous in that beam extraction is not limited by space-charge effects as is the case in gridded ion engines.[2] Many important physical mechanisms of the HET discharge are not yet fully understood, most crucially the mechanisms that govern electron mobility across the magnetic field.

This work refers to experimental HET architectures, in which wall electrodes are employed, as shown in Fig. 1(b). The nominal HET shown in Fig. 1(a) uses a pure dielectric discharge channel (commonly referred to as the magnetic layer or Stationary Plasma Thruster, SPT), which is the most common configuration. There are also HETs that employ a short metallic discharge channel, a configuration called the Thruster with Anode Layer or TAL.[3] HETs with wall electrodes are conceptually in-between SPTs and TALs. A sample electrical circuit schematic for a HET with wall electrodes is shown in Fig. 2. The schematic shows the wall electrodes biased above the anode potential, however, in practice, they may be set to any desired voltage. In this way, wall electrodes add flexibility of operation to the thruster.

Wall electrodes can affect the HET plasma in a variety of ways. The conductive wall electrode material differs from the dielectric channel wall material and thus modifies the secondary electron emission (SEE) from the channel wall. Recent kinetic simulations[4,5] and theoretical investigation[6] have shown that strong SEE from dielectric walls can cause the Debye sheaths at the wall to disappear and even reverse in polarity. Conductive wall electrodes generally have lower SEE yields than the ceramic channel segments they replace, so it is unlikely that introduction of wall electrodes will passively precipitate sheath disappearance when it would not otherwise occur in the SPT. However, if wall electrodes lower the overall SEE to the plasma, the decreased flux of low-energy electrons can lead to increased electron temperature (T_e) in the bulk plasma.

In addition to these passive effects (occurring simply due to the presence of the conductive wall material segment), wall electrodes can create additional effects when biased as part of the thruster circuit. These effects are dependent on the electrode bias potential as well as their axial location and their width along the discharge channel. The HET plasma is denser and more energetic in the region where the Hall current exists, which is typically near the

a)Author to whom correspondence should be addressed. Electronic mail: samuel.langendorf@gatech.edu
b)Electronic mail: gabe.xu@uah.edu
c)Electronic mail: mitchell.walker@ae.gatech.edu

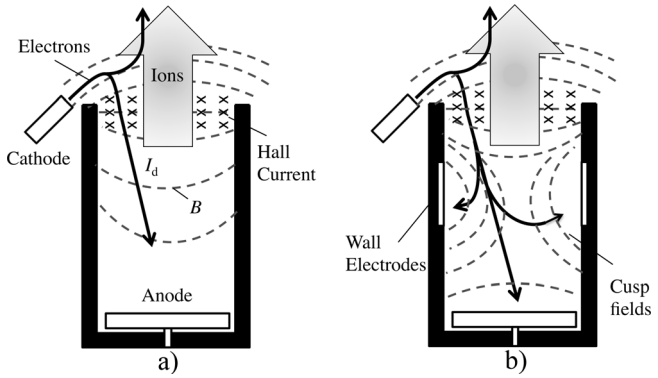

FIG. 1. (a) Diagram of typical HET discharge channel cross section. Discharge current I_d is carried by electrons from cathode to anode. (b) Diagram of HET discharge channel with experimental wall electrodes. Cusp-shaped magnetic fields shown, shaped to decrease electrode current to wall electrodes.

discharge channel exit plane. Plasma densities and electron temperatures are largest in this region. A wall electrode positioned in this region will have the greatest ability to draw electron current from the plasma due to the increased plasma density and electron temperature. Ions incident on the wall in this region may be energetic if they have been radially accelerated by the electric field. Further upstream in the HET discharge channel (closer to the anode), the plasma is less dense and accelerating electric fields are less strong. A wall electrode positioned here will have less ability to draw electron current from the plasma due to the decreased density.

A. Prior research

Some motivations for investigating HETs with wall electrodes are noted by Fruchtman *et al.*[7] For wall electrodes positioned near to the anode, they recognize the possibility to improve HET efficiency if wall electrodes can keep the plasma potential high at near-anode potential throughout the bulk of the channel, as the propellant atoms become ionized. The propellant would then receive the full energy gain of the

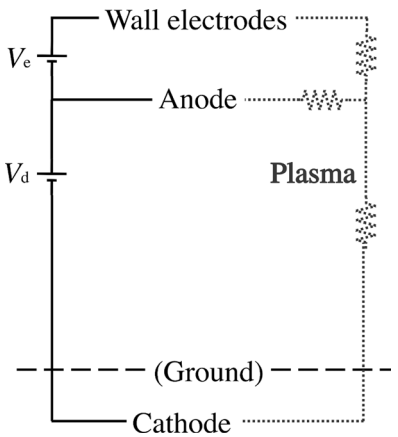

FIG. 2. Electrical schematic for HET with wall electrodes (omitting filter electronics). Electron current flow through the thruster plasma (dotted) completes the circuit. In laboratory experiments, in grounded vacuum chambers, the cathode typically floats below ground as shown.

accelerating potential fall of the discharge at the exit of the channel. Another possible approach is to position wall electrodes close to the exit plane of the thruster, where ions are more likely to be accelerated into the wall, and biasing them above the local plasma potential, thereby focusing the ion plume and decreasing ion wall losses.

Raitses *et al.*[8–10] performed parametric experiments with wall electrodes located near the exit plane in pursuit of these benefits, with mixed outcomes. Kieckhafer[11] investigates a HET with wall electrodes positioned closer to the anode in an attempt to control the amount of current flow to the primary anode. His goal is to modulate the ohmic heating of the anode in order to control the evaporation rate of Bismuth propellant. In separate investigations, Xu[12,13] employs wall electrodes still closer to the anode. These experimental results are discussed below and summarized in Table I.

The results of Raitses *et al.* show that wall electrodes positioned near the exit plane at 0.025–0.3125 of channel length L_c are able to focus the thruster plume and decrease plume divergence, which in isolation is beneficial. However, with only those electrodes installed, the anode efficiency η_a is found to decrease. Anode efficiency (1) disregards any additional power used for electromagnets, cathode heating, and cathode mass flow

$$\eta_a = \frac{0.5\dot{m}_a T^2}{P_d}. \tag{1}$$

In (1), m_a is the anode mass flow rate, T is the thrust, and P_d is the discharge power. The addition of wall electrodes closer to the anode results in mixed beneficial and detrimental impacts to anode efficiency and thrust-to-power ratio (T/P). When calculating η_a and T/P for HETs with wall electrodes, power to the wall electrodes is included in P_d.

Kieckhafer finds that anode efficiency is unaffected by the fraction of current drawn by the wall electrodes, positioned about 0.3 L_c back from the exit plane. While efficiency was unchanged, he found increases in T/P when wall electrodes were biased above the anode.

Xu experimentally investigated a HET with wall electrodes dubbed the Embedded Electrode HET (EEHET), with the wall electrodes positioned 0.58 L_c back from the exit plane, the farthest studied. The EEHET was a modified T-220HT HET to include wall electrodes and additional cusp magnetic fields. The T-220HT has been tested over a range of operating conditions in Ref. 14. Xu altered the magnetic field topography of the thruster to provide cusp-shaped fields over the wall electrodes to reduce their electron current collection. Xu finds a mix of beneficial and detrimental impacts on efficiency as a function of wall electrode bias potential. The largest change to thruster efficiency occurs with the wall electrodes biased 10 V, above anode potential, while at 30 V, above anode potential, they decrease thruster efficiency. This is likely due to the increased electrode power draw that counteracts any thrust gains. Xu also measured the potential contours in the thruster discharge channel with an actuated emissive probe, shown in Fig. 3, with the respective efficiency and T/P measurements shown in Table II. Beam current and energy measurements show that the performance

TABLE I. Summary of prior research.

Reference range	8–10	11	12,13
Number of wall electrodes	1, 2	2	2
Wall electrode material	Rhenium/LaB6	metallic	graphite
Wall electrode SEE	low/high	low	low
Wall electrode location[a]	0.025–0.3125 L_c	~ 0.3 L_c	0.58 L_c
Wall electrode length	0.125–0.050 L_c	~ 0.3 L_c	0.23 L_c
Wall electrode bias	anode, float/cathode	+0–80 V	float, ≥anode
Wall electrode B-field	nominal	nominal	cusped
Operating conditions			
Propellant	xenon	xenon	xenon
Discharge voltages (V)	200–450	300–400	125–300
Discharge currents (A)	1.6–2.8	4–6.5	9, 20
Wall electrode current[b]	0%–9.5%	5%–100%	0%–100%
Mass flow rates (mg/s)	1.7–2.5	4–6	10–22
Performance impacts			
Impact observable when floated	Yes	No	No
Thrust-to-power ratio	−14%–+9%	0%–+15%	0%–+12%
Propellant utilization[c]	−15%–11%	Not measured	0%–+9%
Plume divergence decrease	3°–12°	4°	0°–5°
Anode efficiency (% pts)	−8–+8	Unchanged	−1–+8

[a]Distance from exit plane to center of wall electrode, L_C = discharge channel length.
[b]Percentage of discharge current.
[c]Plume ion current/mass flow rate.

improvements are due to increased ion flux leaving the thruster and not from increased ion velocity.

The current work conducts a theoretical analysis of the EEHET and discusses the combined results of the prior research to give a general picture of wall electrode effects. In Sec. II, the sheath regions of the EEHET plasma are discussed. In Sec. III, the EEHET presheath/bulk plasma regions are discussed and the current flow is simulated using a one-fluid model. In Sec. IV, the conclusions from the EEHET results are discussed in light of the prior research.

II. EEHET SHEATH EFFECTS

If the wall electrodes are biased above the local plasma potential, one might expect them to behave similarly to a positive-biased Langmuir probe, i.e., to collect electron current and repel ions, as desired. However, if the electrodes collect all of the electron current of the thruster discharge, further increases in the wall electrode potential do not result in increased sheath potentials and ion repulsion but instead in increased local plasma potential. In this way, the wall

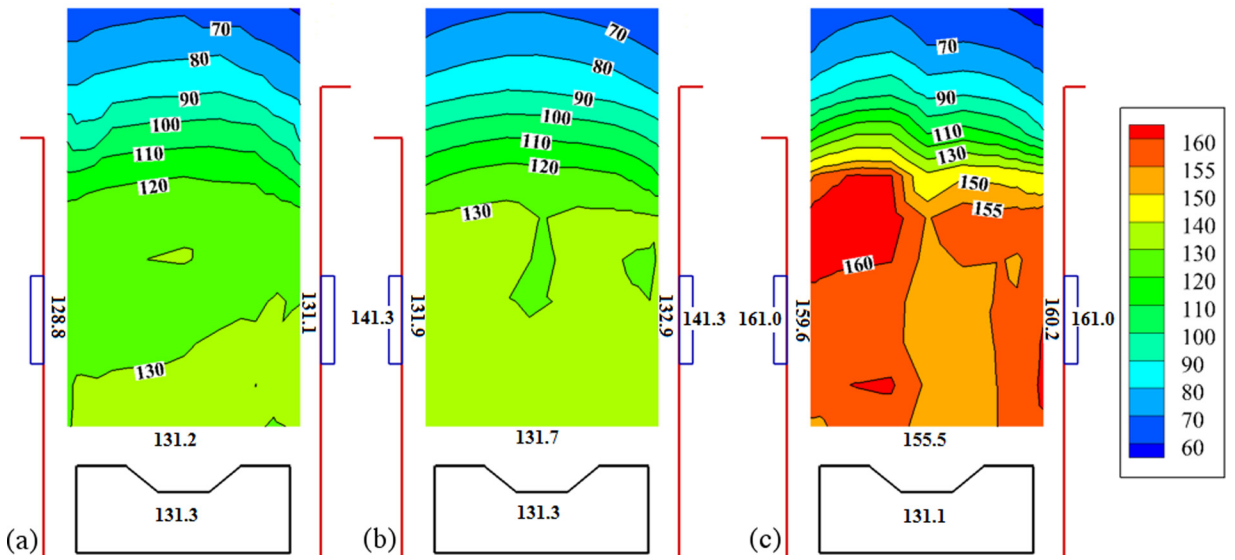

FIG. 3. Discharge channel plasma potential measurements with respect to ground (V) obtained in HET with wall electrodes, with a floating emissive probe. Centerline is to the right, magnetic field is kept constant. In case (a), the wall electrodes are floating. In cases (b) and (c), the wall electrodes are biased 10 V and 30 V above the anode, respectively. The applied discharge voltage (V_d) on the anode with respect to the cathode is 150 V in each case. Thus, in (b) and (c) the electrodes are at 160 and 180 V with respect to the cathode. Discharge current (I_d) is held at 9 A by adjustment of xenon flow rate, to 11.04 mg/s in case (a), 10.34 mg/s in case (b), and 11.01 mg/s in case (c).[12]

TABLE II. Measurements of thruster efficiency, current, and sheath potential for experimental cases in Fig. 3 for $V_d = 150$ V, $I_d = 9$ A, and xenon propellant. A control case with BN walls was not run with xenon but was run with Krypton propellant, which showed no significant changes in performance or floating potential contours.[12]

	(a)	(b)	(c)
Anode efficiency (%)	19.5	24.8	23.2
Thrust/power (mN/kW)	56.5	61.1	55.7
Discharge current (A)	−8.90	−9.08	−8.93
Wall electrode current (A)	0.00	1.55	9.35
Anode current (A)	1.38	7.53	−0.42
Anode sheath (V)	−0.1 ± 5	+0.4 ± 5	24.5 ± 5
Wall electrode sheath (V)	…	+8.9 ± 5	+1.1 ± 5

electrodes can take on the role of a primary anode in the thruster discharge. In Sec. II A, measured sheath potentials in the EEHET are discussed in more detail. In Sec. II B, the criterion for ion-repelling wall electrode sheath formation is discussed. In Sec. II C, the current collection by the wall electrodes across magnetic field is discussed.

A. Sheath potentials

The cathode-to-ground voltage is available in Ref. 12 for the measurements in Fig. 3, as well as the discharge voltage from cathode to anode and from wall-electrodes-to-anode. This allows us to back out the wall electrode potentials with respect to ground in each case and add the labels in Fig. 3 (except for case (a), in which the wall electrode floating voltage is not available). We compute the anode sheath potential and wall electrode sheath potential in Table II by subtracting the mean of the measured local plasma potentials. A control case with fully dielectric walls was not run with xenon, but was run with krypton propellant, which showed no changes in performance or floating potential contours. This differs from the results of Raitses *et al.,* wherein the passive presence of the wall electrodes caused a change in anode efficiency. The difference is attributable to the position of the wall electrodes farther back from the dense, energetic plasma of the Hall current region, so the change in SEE from the material is less influential.

The anode potentials lie both above and below the local plasma potentials, depending on operating condition. This agrees with expectations from SPT studies—for a conventional SPT, Dorf *et al.*[15] show that the anode sheath can be either electron-attracting or electron-repelling, depending on the thruster dimensions and operating conditions. The reason is that the propellant flow rate, discharge voltage, and magnetic field control the discharge current and the plasma density near the anode. If the thermal electron flux is greater than the discharge current (I_d), the sheath must be electron-repelling. If this flux is less than I_d, the sheath must be electron-attracting. In a HET with wall electrodes, this same logic is applicable, with the consideration that the discharge current is shared amongst all of the plasma-facing electrodes.

When the wall electrodes are biased 10 V above the anode (Fig. 3(b)), they sustain electron-attracting (and hence ion-repelling) sheaths. This is also the condition when the best efficiency and thrust-to-power ratio is observed. When the wall electrodes are biased 30 V above the anode, the sheath potential is once again within experimental error (Fig. 3(c)). The loss of the performance benefits in case (c) suggest that the electron-repelling anode sheath is due to the decrease in the electron current to the anode as it preferentially travels to the wall electrodes.

In Table II, case (b) is the only case in which an ion-repelling sheath unambiguously exists over the wall electrodes, and this is also the case where efficiency and T/P improvements are observed (cf. Table II). Data from the same thruster across a range of discharge voltages display a negative correlation between electrode current draw and T/P, as shown in Fig. 4. This supports the idea that once the majority of incident ions are repelled, any further increases in electrode bias potential only results in increased electron current collection and thus power draw, which decreases the T/P.

B. Sheath polarity

The only condition under which an ion-repelling sheath can form is if the electron loss to the surface is kept below the ion loss rate of the system by some means. Due to the large mass difference between electrons and ions, electron fluxes are much larger, thus, sheaths are commonly electron-repelling to maintain quasineutrality. Ion-repelling sheaths are seen in Langmuir probes because the probe tip represents a very small fraction of the total plasma volume, limiting its electron current draw. In the EEHET, ion-repelling sheaths exist on the wall electrodes due to the application of cusp-shaped magnetic fields to reduce their electron current draw.

Ion losses in Hall thrusters come from multiple sources: ions being accelerated into the plume to produce thrust, wall losses, and recombination in the plasma. The loss of ions from acceleration into the plume is the most significant, so one can approximate the ion loss rate L_i by the beam current, which is typically slightly less than the discharge current

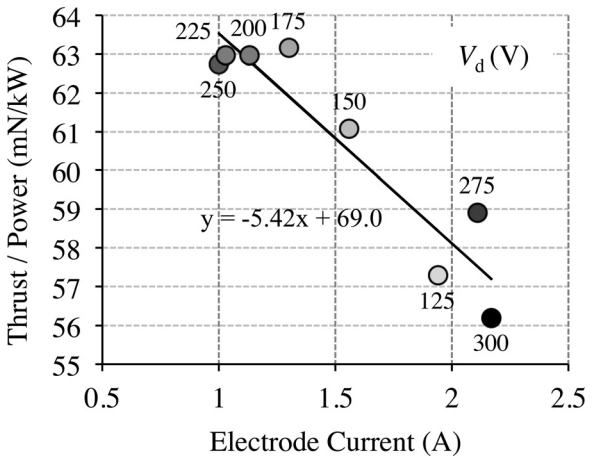

FIG. 4. T/P vs. wall electrode current for the 9 A xenon data of Ref. 12 with wall electrodes biased +10 V to anode for many discharge voltages. Data are negatively correlated ($r = -0.935$) due to the increase in overall thruster power draw (wall electrodes draw an increased amount of the discharge current, biased ($V_d + V_c$) above cathode > anode biased V_d above cathode).

$$L_i \approx \frac{I_b}{e} \approx \frac{I_d}{e}. \quad (2)$$

Consequently, a probe-like ion-repelling sheath is not able to form over an electrode that collects the dominant fraction of the discharge current. This gives a useful criterion for the design of wall electrodes, in which the goal is to achieve probe-like biases that do not affect the bulk plasma potential: The collected current by the wall electrode (I_{we}) must be substantially less than the discharge current

$$I_{we} \ll I_b. \quad (3)$$

This is in agreement with the EEHET results, which show that the ion-repelling sheaths over the wall electrodes vanish when the wall electrodes come to collect the bulk of the discharge current (Fig. 3(c)) and the local plasma potential nominally increases to within 1.1 V of the wall electrode potential.

C. Current draw

Because the electron current collected by the wall electrodes must be kept below the ion loss rate in order for them to exhibit an ion-repelling sheath, and thus improve thruster performance, it is of interest to be able to predict the current draw to the electrodes. The current collected by the electrode is the flux that arrives from the plasma at the sheath edge (neglecting reflection and SEE) so, in general, changes in sheath thickness can affect current draw. In the planar geometry, this is limited to edge effects. In Bohm,[16] a case is treated for a thin disc-shaped probe in a magnetic field parallel to the probe surface. It is shown that the sheath volume of the probe is compressed in the field normal direction, but elongated in the field tangential direction due to the preferential electron mobility along the magnetic field. In this way, with a magnetic field parallel to a finite planar electrode surface, the electrode is able to collect current from beyond its physical extent in the tangential direction as the sheath expands. Bohm shows that the expansion in the tangential direction should scale with $B^{1/2}$, where B is the magnetic field strength.

Electron mobility in HETs results from multiple mechanisms: in the near-anode region mobility is dominated by classical collisional diffusion, while in the Hall current region near the channel exit plane the mobility is much greater than classical. This increased "anomalous" mobility has been attributed primarily to fluctuation-induced Bohm transport. The EEHET wall electrodes and cusp magnetic fields are positioned in the ionization zone, where both mechanisms can be expected to be significant. Classical transport scales as B^{-2} and Bohm transport as B^{-1}, so the current collection to the electrode should scale as $B^{-1/2}$ to $B^{-3/2}$.

In the EEHET, the magnetic field is not parallel to the wall electrode, but cusp-shaped, so deviation from the $B^{-1/2}$ model of sheath expansion is expected. In the EEHET, there are separate magnetic coils that provide the cusp-shaped field over the wall electrodes, so it is possible to observe the current collection as the shielding field is increased. A $B^{-1/2}$ scaling qualitatively agrees with the experimental observation, as shown in Fig. 5, but the measurements indicate that from 10 to 15 A cusp magnet current, there is no appreciable decrease in electrode current (rather, a small increase.) This could indicate that the expansion of the sheath area caused by the magnetic field has become more significant than the reduction in cross-field mobility. In particular, if the sheath is able to expand downstream into the denser plasma near the HET exit plane, the collected current could increase faster than predicted and account for the observation.

In summary, wall electrodes can repel low-temperature ions when they are positioned far back from the exit plane, to the benefit of the thruster performance. Ion-repelling sheaths are able to form if the electron current they collect is kept much lower than the discharge current. However, if the wall electrodes are allowed to collect significant current and become the primary anodes of the discharge, they control the local plasma potential and thus affect the potential structure of the entire discharge. To investigate this effect, one must consider the behavior of the bulk plasma, which is the focus of Sec. III.

III. EEHET PRESHEATH/BULK PLASMA

The transition between a quasineutral plasma and an ion-attracting sheath requires a presheath, a potential drop sufficient to accelerate ions to the Bohm speed and establish the non-quasineutral sheath region. For a relatively thin plasma volume, such as the annular discharge channel of the HET, the smallest length scale determining the presheath thickness is the width of the channel itself,[17] so the presheath is encompassing the whole channel. In the floating case Fig. 3(a), the potential contours are convex and accelerate ions towards the wall, thus fulfilling the role of the presheath. At high wall electrode bias, "pockets" of high potential near the wall electrodes and inward-radial electric fields are observed in the bulk plasma (cf. Fig. 3(c)), contrary to the normal presheath expectation. This type of presheath could be consistent with the predictions of Beilis,[18] who find that presheaths may reverse polarity depending on the ratio of current

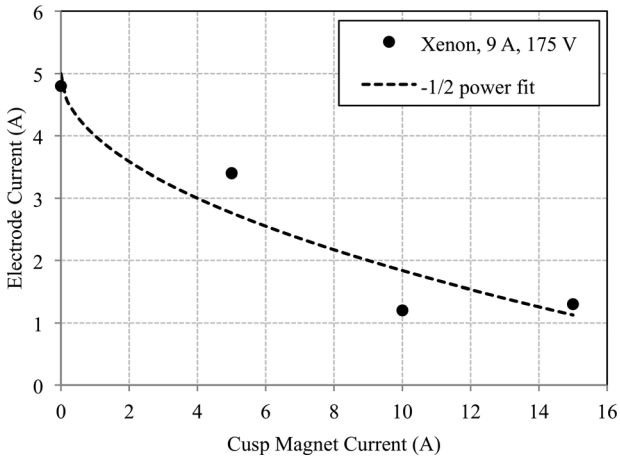

FIG. 5. Experimental observation of current collection by wall electrodes and $B^{-1/2}$ fit. The abscissa indicates current to a set of magnetic coils designed to generate cusp-shaped fields to shield the wall electrodes.

collected. It is also supported by the recent theory of ion-repelling sheaths by Campanell,[6] who argues that the Bohm criterion is not needed when the sheath is a single layer of negative space charge. The inward-radial E-fields are only observed when there is current draw to the wall electrodes, to a small degree in Fig. 3(b) and more so in Fig. 3(c). The data show that positive-biased wall electrodes can change the potential structure in the channel such that a traditional ion-accelerating presheath does not form, at the cost of drawing electron current from the plasma.

A. Fluid model of electron transport

In order to isolate and examine the proposed mechanism for the formation of in-channel electric fields, a one-fluid model is applied to a 2D domain of the EEHET discharge channel. Despite the recent application of high-fidelity particle-in-cell methods to HET modeling,[19,20] the 2D one-fluid model is selected to provide a reduced subset of physics and reduced computational time to investigate the potential structures. An "exit plane" potential boundary condition is placed at the channel exit plane, and current flow is calculated to an anode and two wall electrodes. The model setup is illustrated in Fig. 6.

The HET discharge current is carried by electrons, resulting in the Ohm's law formulation[21]

$$J_e = \sigma(\vec{E} + \nabla T_e + T_e \nabla \ln n_e) + \mu(\vec{J}_e \times \vec{B}). \tag{4}$$

In (4), J_e is the electron current, σ is the conductivity, and μ is the electron mobility. Conductivity and mobility are defined with an effective collision frequency equal to the sum of collisional (ν_e) and Bohm (ν_B) frequencies

$$\sigma = \mu n_e e = \left(\frac{e}{m_e \nu_e}\right) n_e e = \frac{n_e e^2}{m_e(\nu_c + \nu_B)}. \tag{5}$$

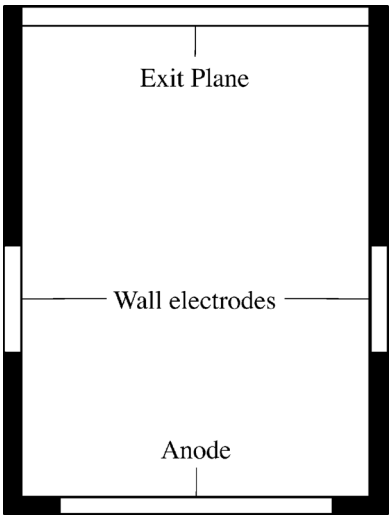

FIG. 6. Model domain of HET discharge channel section. Shaded regions are dielectric channel wall segments, with floating potential boundary condition. Unshaded regions show locations of wall electrode, anode, and exit plane potential boundary conditions.

TABLE III. Model inputs and boundary conditions.

	(a)	(b)	(c)
Exit plane potential BC (V)	91.1	94.6	99.4
Wall electrode potential BC (V)	131.1	132.4	159.9
Anode potential BC (V)	131.2	131.7	155.5
Channel wall current BC (A)	0	0	0

Near-wall mobility enhancements are neglected. Due to magnetic field, conductivity is anisotropic in the channel reference frame but diagonal in the reference frame of the magnetic field lines, so a transformation is used following Ref. 19 that permits the model description to remain in channel coordinates

$$j_z = \mu_{11}\sigma(E_z + \nabla_z T_e + T_e \nabla_z \ln n_e) + \mu_{12}\sigma(E_r + \nabla_r T_e + T_e \nabla_r \ln n_e), \tag{6}$$

$$j_r = \mu_{21}\sigma(E_z + \nabla_z T_e + T_e \nabla_z \ln n_e) + \mu_{22}\sigma(E_r + \nabla_r T_e + T_e \nabla_r \ln n_e), \tag{7}$$

$$\begin{bmatrix} \mu_{11} & \mu_{12} \\ \mu_{21} & \mu_{22} \end{bmatrix} = \frac{1}{(1+\mu^2 B^2)} \begin{bmatrix} (1+\mu^2 B_z^2) & \mu^2 B_z B_r \\ \mu^2 B_r B_z & (1+\mu^2 B_r^2) \end{bmatrix}. \tag{8}$$

The system of (4)–(8) is implemented in 2D in the finite element software COMSOL Multiphysics (formerly FEMLAB) electric currents module, which supplies the additional element-wise equations to enforce current conservation and compute scalar potential

$$\nabla \cdot j - Q_j, \tag{9}$$

$$E = -\nabla V, \tag{10}$$

in which Q_j is the element-wise current density. The thruster magnetic field is imported from a cross-section of the thruster 3D magnetic field model created in Infolytica's MagNet software. Inputs and boundary conditions are listed in Table III. The model does not include space charge effects or sheaths, so the electrode bias voltages in the model are taken as the sheath edge potentials as previously determined in Table II. In addition, any sheath expansion is neglected. The exit plane potential boundary condition is set to the mean of the measured values. A constant electron density of

TABLE IV. Model predictions of current distribution between electrodes. Current densities per unit length (out-of-plane) are multiplied by HET mid-channel diameter to obtain estimates of current to each electrode.

	(a)	(b)	(c)
Exit plane current (A)	−1.38	−1.27	−1.93
Wall electrode current (A)	0.00	0.29	1.65
Anode current (A)	1.38	0.99	0.28
Wall electrode current (%)	0	23	85
Anode current (%)	100	78	15
Measured wall electrode current (%)	0	17	105
Measured anode current (%)	100	83	−5

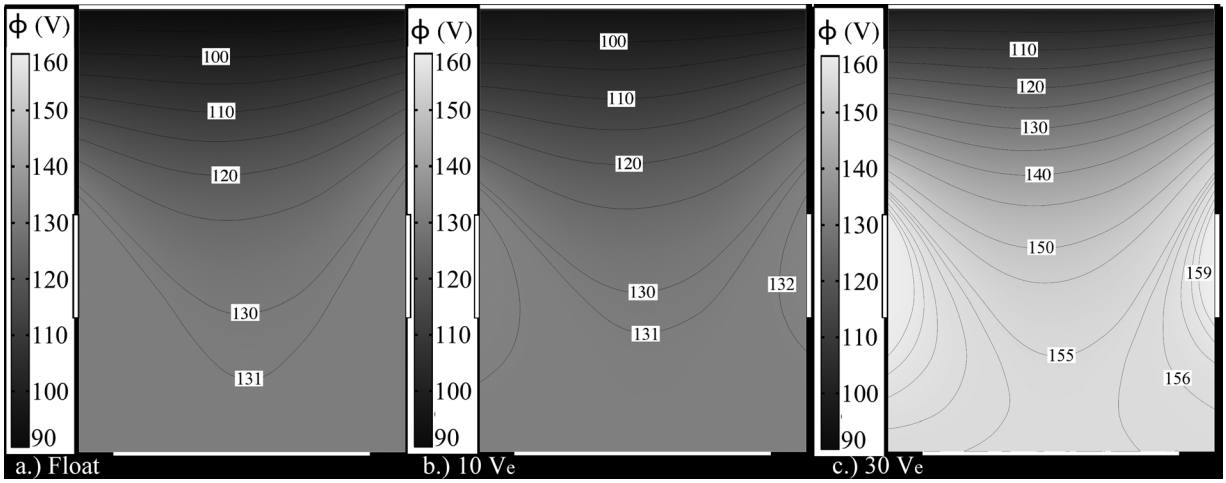

FIG. 7. Model results of electric potential, based on input conditions from experimental measurements in the EEHET. Case (a) mimics the experimental case with floating wall electrodes, case (b) mimics the +10 V bias above anode potential wall electrodes, and case (c) the +30 V bias. Wall electrode position shown by unshaded wall segments. Black lines represent electric potential contours. Input conditions are listed in Table III, from data of Fig. 3.

$10^{17}\,m^{-3}$ and an electron temperature of 15 eV are assumed in agreement with a theoretical estimate in Ref. 13, and electron temperature measurements. The mesh is refined until grid independence is achieved as <0.5% variation in the current to each electrode per 10 000 additional elements. The computational time for each case is about 20 s on a 2.2 GHz virtual machine with 4 GB RAM.

Model results are shown in Figs. 7 and 8 for the input cases of Table III, chosen to mimic the experimental cases of Fig. 3/Table II. The output values of the current drawn by each electrode in each case are listed in Table IV.

The potential contours present in the model show the formation of high potential pockets near the wall electrodes when they are biased positively relative to the anode (cf. Fig. 7(c)). This agrees with experimental observations in Fig. 3. With floating/low wall electrode biases, the cusp-shaped fields are able to shield the wall electrodes and the bulk of the current flows to the anode (cf. Figs. 8(a) and 8(b)). As the wall electrode bias voltage is increased, the wall electrodes collect most of the current and become the primary anode of the thruster discharge. The in-channel focusing radial electric fields then become more prominent at the higher electrode bias, as seen in both the experimental and modeling results.

The model does not treat the thruster ions, and thus excludes presheath effects. The potential contours in the model closely follow the magnetic field contours, without having to provide ions with a potential drop to reach the Bohm velocity at the wall. The resulting predictions are closer to the experimentally measured potential contours of Fig. 3 for the case of +30 V wall electrodes, in keeping with the reasoning that the wall electrodes have established ion-repelling sheaths and thus do not create a traditional ion-accelerating Bohm presheath.

The current sharing by the electrodes (Table IV) shows similar proportions to the experimental result, although the magnitude is decreased by almost an order of magnitude. This is most likely a result of inaccuracy in the assumed

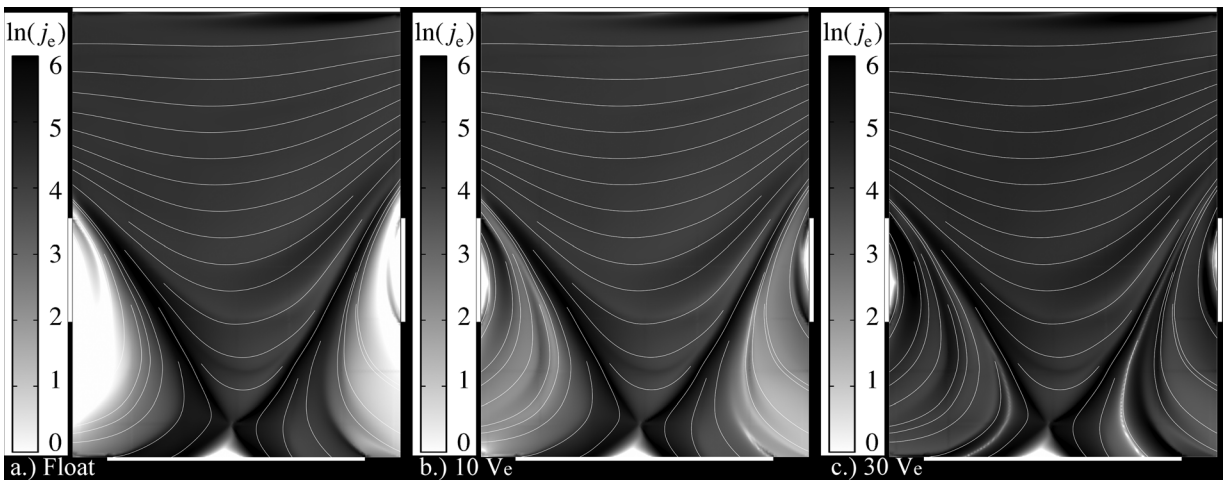

FIG. 8. Model results of current density, based on input conditions from experimental measurements in the EEHET. Position of wall electrodes shown by unshaded wall segments. White lines represent magnetic field lines, shading is natural logarithm of current density. Input conditions listed in Table III, from data of Fig. 3. In the low bias case (a), wall electrodes are shielded by the magnetic field.

electron number density and electron mobility. However, the agreement in current sharing fractions is promising, as this could help in predicting the types of sheaths achievable (recalling from (3) that wall electrode current must be much less than the discharge current to be able to bias the wall electrode independently of the local plasma and achieve ion-repelling sheaths).

IV. CONCLUSIONS

The analysis of the EEHET contributes to understanding of wall electrode effects gathered from previous researchers (Table I). It is found that ion-repelling sheaths over the wall electrodes are correlated with performance benefits in the EEHET. Ion-repelling sheaths are achieved with the wall electrodes positioned in the near-anode region of the EEHET, but it is unlikely that this can be achieved in the dense plasma region where the electron temperature is higher, the current collected from the plasma for a given sheath voltage is much greater, and the incident ions are more energetic.

The positive bias of the wall electrodes is able to change the potential structure over the whole discharge channel/pre-sheath. For the purposes of the EEHET, the best efficiency is achieved by a slight increase of the wall electrodes above anode potential, which alleviates the requirement for the Bohm presheath and changes the potential structure to guide ions away from the wall and into the acceleration region near the channel exit plane.

Perhaps, the most important conclusion from this analysis is that ion-focusing electric fields in the presheath/bulk plasma accomplished by wall electrodes are fundamentally linked with the electron current they draw. If wall electrodes are positioned too near the exit plane, they will not be able to repel ions accelerated at the wall without drawing the bulk of the discharge current and short-circuiting the discharge, decreasing thruster efficiency. They show some effectiveness when located further upstream in the discharge channel by preventing early ion loss to the wall, but do not affect the potential contours in the most important dense plasma region near the exit plane, and therefore, it is unlikely that wall electrodes as currently envisioned will be able to achieve a beam-focusing effect that does not sacrifice thruster efficiency.

ACKNOWLEDGMENTS

This work was supported by Moog In-Space Propulsion. The authors thank Lake A. Singh, Natalie R. Schloeder, Scott T. King, and Jason D. Frieman for helpful discussions.

[1]E. Y. Choueiri, A. J. Kelly, and R. G. Jahn, "Mass savings domain of plasma propulsion for LEO to GEO transfer," J. Spacecr. Rockets **30**(6), 749–754 (1993).
[2]D. M. Goebel and I. Katz, *Fundamentals of Electric Propulsion: Ion and Hall thrusters* (John Wiley & Sons, Hoboken, New Jersey, 2008), Vol. 1.
[3]V. V. Zhurin, H. R. Kaufman, and R. S. Robinson, "Physics of closed drift thrusters," Plasma Sources Sci. Technol. **8**(1), R1 (1999).
[4]D. Sydorenko, I. Kaganovich, Y. Raitses, and A. Smolyakov, "Breakdown of a space charge limited regime of a sheath in a weakly collisional plasma bounded by walls with secondary electron emission," Phys. Rev. Lett. **103**(14), 145004 (2009).
[5]M. D. Campanell, A. V. Khrabrov, and I. D. Kaganovich, "General cause of sheath instability identified for low collisionality plasmas in devices with secondary electron emission," Phys. Rev. Lett. **108**(23), 235001 (2012).
[6]M. D. Campanell, "Negative plasma potential relative to electron-emitting surfaces," Phys. Rev. E **88**(3), 033103 (2013).
[7]A. Fruchtman, N. J. Fisch, and Y. Raitses, "Hall thruster with absorbing electrodes," in Proceedings of the 36th AIAA/ASME/SAE/ASEE Joint Propulsion Conference, AIAA-2000-3659, Huntsville, Alabama, 17–19 July 2000.
[8]N. J. Fisch, Y. Raitses, A. A. Litvak, and L. A. Dorf, "Design and operation of Hall thruster with segmented electrodes," AIAA Paper 99-2572, 1999.
[9]Y. Raitses, L. A. Dorf, A. A. Litvak, and N. J. Fisch, "Plume reduction in segmented electrode Hall thruster," J. Appl. Phys. **88**(3), 1263–1270 (2000).
[10]N. J. Fisch, Y. Raitses, L. A. Dorf, and A. A. Litvak, "Variable operation of Hall thruster with multiple segmented electrodes," J. Appl. Phys. **89**(4), 2040–2046 (2001).
[11]A. W. Kieckhafer, "The effect of segmented anodes on the performance and plume of a Hall thruster," Ph.D. dissertation (Michigan Technological University, 2007).
[12]K. G. Xu, "Ion collimation and in-channel potential shaping using in-channel electrodes for Hall effect thrusters," Ph.D. dissertation (Georgia Institute of Technology, 2012).
[13]K. G. Xu, H. Dao, and M. L. R. Walker, "Potential contour shaping and sheath behavior with wall electrodes and near-wall magnetic fields in Hall thrusters," Phys. Plasmas **19**, 103502 (2012).
[14]S. F. Engelman, F. S. Gulczinski, E. J. Beiting, and J. E. Pollard, "Characteristics of the T-220HT Hall-effect thruster," in Proceedings of the 39th AIAA/ASME/SAE/ASEE Joint Propulsion Conference, AIAA Paper 2003-5158, 20–23 July 2003, Huntsville, AL.
[15]L. Dorf, V. Semenov, and Y. Raitses, "Anode sheath in Hall thrusters," Appl. Phys. Lett. **83**(13), 2551–2553 (2003).
[16]D. Bohm, "Minimum ionic kinetic energy for a stable sheath," in *The Characteristics of Electrical Discharges in Magnetic Fields*, edited by A. Guthrie and R. K. Wakerling (McGraw-Hill, New York, 1949), pp. 77–86.
[17]M. Gamero-Castano and I. Katz, "Estimation of Hall thruster erosion using HPHall," in Proceedings of the 29th International Electric Propulsion Conference, IEPC-2005-303 (2005).
[18]I. I. Beilis, M. Keidar, and S. Goldsmith, "Plasma-wall transition: The influence of the electron to ion current ratio on the magnetic presheath structure," Phys. Plasmas **4**(10), 3461–3468 (1997).
[19]F. Taccogna, S. Longo, M. Capitelli, and R. Schneider, Contrib. Plasma Phys. **47**(8–9), 635–656 (2007).
[20]J. Pérez-Luna, N. Dubuit, L. Garrigues, G. Hagelaar, and J. P. Boeuf, "Electron trajectories in a Hall effect thruster anomalous transport induced by an azimuthal wave," IEEE Trans. Plasma Sci. **36**(4), 1212–1213 (2008).
[21]J. Geng, L. Brieda, L. Rose, and M. Keidar, "On applicability of the 'thermalized potential' solver in simulations of the plasma flow in Hall thrusters," J. Appl. Phys. **114**(10), 103305 (2013).